GEOPHYSICS, VOL. 79, NO. 4 (JULY-AUGUST 2014); P. B135–B149, 17 FIGS., 4 TABLES.
10.1190/GEO2013-0268.1

Case History

Detailed topography of the Devonian Grosmont Formation surface from legacy high-resolution seismic profiles, northeast Alberta

Elahe P. Ardakani[1], Douglas R. Schmitt[1], and Todd D. Bown[1]

ABSTRACT

The Devonian Grosmont Formation in northeastern Alberta, Canada, is the world's largest accumulation of heavy oil in carbonate rock with estimated bitumen in place of 64.5×10^9 m^3. Much of the reservoir unconformably subcrops beneath Cretaceous sediments. This is an eroded surface modified by kartstification known as the Sub-Mannville Unconformity (SMU). We studied the reanalysis and integration of legacy seismic data sets obtained in the mid-1980s to investigate the structure of this surface. Standard data processing was carried out supplemented by some more modern approaches to noise reduction. The interpretation of these reprocessed data resulted in some key structural maps above and below the SMU. These seismic maps revealed substantially more detail than those constructed solely on the basis of well-log data; in fact, the use of only well-log information would likely result in erroneous interpretations. Although features smaller than about 40 m in radius cannot be easily discerned at the SMU due to wavefield and data sampling limits, the data did reveal the existence of a roughly east–west-trending ridge-valley system. A more minor northeast–southwest-trending linear valley also was apparent. These observations are all consistent with the model of a karsted/eroded carbonate surface. Comparison of the maps for the differing horizons further suggested that deeper horizons may influence the structure of the SMU and even the overlying Mesozoic formations. This suggested that some displacements due to karst cavity collapse or minor faulting within the Grosmont occurred during or after deposition of the younger Mesozoic sediments on top of the Grosmont surface.

INTRODUCTION

The Devonian Grosmont Formation of the northeastern Alberta plains is a carbonate platform encompassing an area of 85,000 km^2, of which about 20,800 km^2 is prospective for bitumen (Figure 1a). Many authors have indicated that the area of the Grosmont platform is comparable to that of the modern-day Bahama Banks (Figure 1b). This may also be a reasonable geologic analog in that, even though much of the Bahama Banks is currently submerged, during recent glacial maxima, it was dry land subject to karsting.

The Grosmont Formation is projected to hold upwards of 64.5×10^9 m^3 of bitumen according to the recently updated reserves estimates of the Energy Resources Conservation Board (2010). In the past decade, there has been a great deal of interest in exploiting this resource. However, this is only the second round of investigation of the Grosmont reservoir. In the early to mid 1980s, the reservoir was first tested in a government/industry project supported through the Alberta Oil Sands Technology and Research Authority (AOSTRA). This consortium acquired geophysical and well-log data and initiated a few pilot project tests. Much of the geologic information, primarily from well logs and cores, has already been published from various sources and entered into the public record (Belyea, 1956; Dembicki and Machel, 1996; Buschkuehle et al., 2007; Barrett and Hopkins, 2010; Borrero and Machel, 2010; Machel, 2010; Wo et al., 2010; Machel et al., 2012); however, the abrupt termination of the research project related to the decline of heavy hydrocarbon prices in the late 1980s together with the general lack of now-ubiquitous computer-assisted interpretation programs did not allow for proper integration of all of the seismic data obtained in the research.

Manuscript received by the Editor 16 July 2013; revised manuscript received 22 December 2013; published online 4 June 2014; corrected version published online 12 June 2014.
[1]University of Alberta, Department of Physics, Edmonton, Alberta, Canada. E-mail: e.poureslami@ualberta.ca; dschmitt@ualberta.ca; tbown@ualberta.ca.

The primary purpose of this contribution is to illustrate using seismic data the complexities of the eroded and karsted Grosmont surface; such detail cannot be achieved from the sparse sampling available from direct borehole measurements. Secondarily, the contribution seeks to preserve a unique and perhaps historic geophysical data set. The 2D seismic data obtained here cannot hope to compete against modern 3D seismic imaging. However, the researchers attempted to push the limits in terms of improving the ability to resolve the shallow Grosmont surface, and the "high-spatial-resolution" sampling they finally adopted was unique for the time period and hints toward more modern data acquisition strategies. The data obtained clearly illustrate the evolution of technique over this time period as the researchers were forced to concede that standard practices could not work well in imaging the relatively shallow unconformity surface. The contribution begins with information on the current state of knowledge as to the regional and more local geologic structure. The legacy data are then presented in detail and the reprocessing and integrated strategies described. Interpretation of the integrated seismic data allows for a relatively detailed mapping of the Grosmont surface over the study area that displays substantial topographic variations likely related to karst-driven erosion.

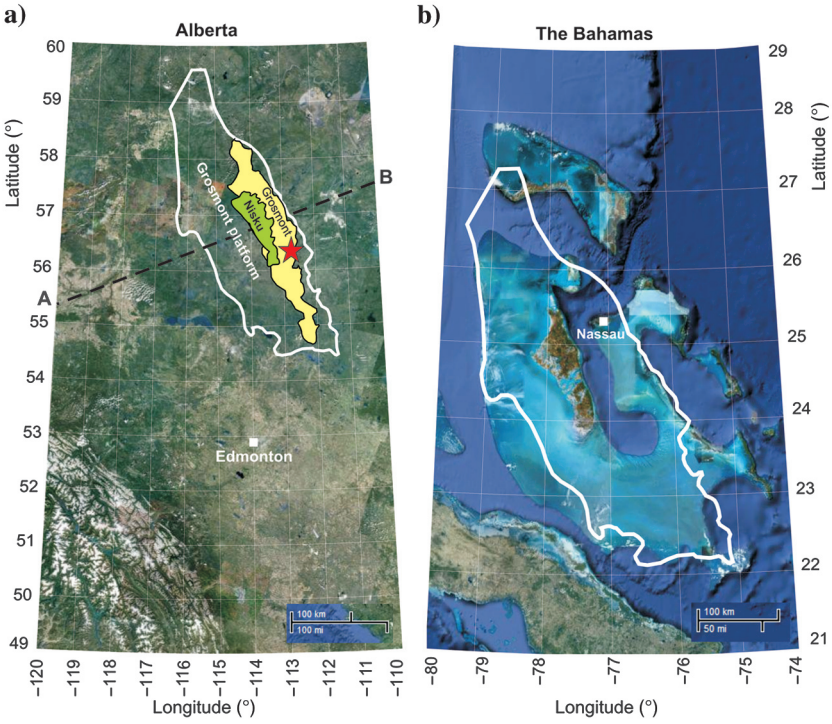

Figure 1. (a) Satellite image of Alberta showing the extent of the Grosmont platform in white. Outlines of the areas of the Grosmont and Nisku carbonate bitumen deposits in yellow and green, respectively. The area of study is shown with the red star. (b) Satellite image of the Bahama Banks illustrating the size of a modern-day shallow-water carbonate platform. Outline of the Grosmont platform from Figure 1a superimposed in white. Images from NASA (NASA, 2012).

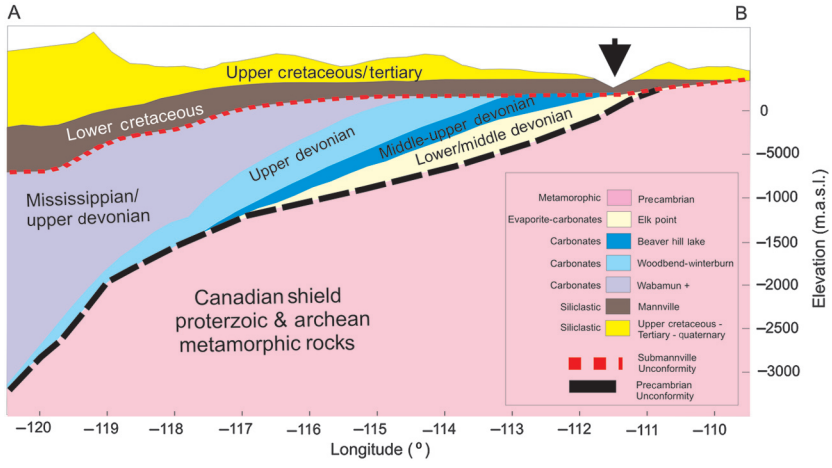

Figure 2. Synoptic cross section A-B (outlined in Figure 1a with the dashed line) shows the general geologic structure around the study area (black arrow) developed from digital geologic formation tops, from Mossop and Shetsen (1994).

Regional geology

The gross geologic structure of Alberta, east of the disturbed belt and Rocky Mountains consists of a wedge of sediments, overlying the Archean and early Proterozoic metamorphic rocks of the Canadian Shield. The sedimentary basin is about five or more kilometers thick at its western edge, and it thins progressively northeastward. This veneer of sediments disappears entirely in the extreme northeastern corner of Alberta where the Canadian Shield is exposed. To the first order, this sediment wedge consists of two major parts. Indurated older sediments with ages ranging from the latest Proterozoic through the Paleozoic with some limited early Mesozoic sediments immediately overlie the Canadian Shield. For a large part, these were marine carbonates and shale deposits laid down on a passive continental margin. The topmost wedge, in contrast, consists of Mesozoic siliciclastic sands and shales deposited in shallow seas and estuarine and fluvial environments.

The geologic unconformity separating the primarily Paleozoic and Mesozoic sediments is a major basinwide feature and plays an important role in this study because the bulk of the bitumen resides at and immediately beneath this interface. The cross section A-B crossing the Grosmont platform (outlined in white) from Figure 1a is shown in Figure 2, which represents the large scale geologic structure representative of the study area. The predominant lithologies within the various sedimentary layers overlying the Canadian Shield begin with the lower Devonian Elk Point Group containing significant evaporates and carbonates, the mid-to-Upper Devonian Beaverhill Lake Group, the Upper Devonian Woodbend-Winterburn Group, and the Upper Devonian and Mississippian Wabamun and other formations. These are all blanketed by the Lower Cretaceous Mannville Group, which is in turn covered by Upper Cretaceous and, in some locales, Tertiary sediments (Figure 2).

Two unconformities are seen here. The first is the unconformity between the Lower Devonian Elk Point and the Pre-Cambrian metamorphic Canadian Shield (PCU). This unconformity separates the rocks in time by more than 1.5 Ga. Although this unconformity will not play a major role in this study, it is important not to forget it because it may hold clues as to the potential for large-scale tectonic motions that could directly via faulting or indirectly via deformation of deeper sedimentary formations eventually influence the Upper Devonian formations being studied here (Cotterill and Hamilton, 1995). The second shallower Sub-Mannville unconformity (SMU) separates the Mesozoic Lower Cretaceous siliciclastic rocks from the Upper Devonian carbonates. This unconformity goes by many different names in the literature (e.g., Sub-Cretaceous, Paleozoic), but here we use Sub-Mannville because in the study area, the Lower Cretaceous Mannville Group covers the subcropping Upper Devonian rocks. This unconformity is the key to the development of the Grosmont resource that abuts the unconformity. The unconformity surface was modified by a combination of erosion and karsting, and this raises numerous complexities to the development of the resource because it remains difficult to delineate smaller karst features.

Local stratigraphy

In the study area, all of the SMU rocks are of Devonian age beginning with various Upper Devonian Nisku, Upper Ireton, and Grosmont Formation subcropping. The Ireton and Grosmont Formations belong to the Upper Devonian Woodbend Group and the Nisku to the Winterburn Group (Switzer et al., 1994). At the scale of the Western Canadian Sedimentary Basin (and even beyond), the Woodbend holds important siliciclastic sources (Duvernay and Muskwa Formations) and reservoir rocks, particularly the large (up to 275 m high) Leduc reef complexes and the generic Grosmont subcropping bitumen reservoirs of interest here. The Woodbend-Winterburn Groups represent rapid deposition of substantial amounts of carbonates and basin-filling shales that exceeds 850 m thickness in some places: a substantial fraction of the basin itself. This occurred over a short period of about only 7 Ma from the early Famennian (375 Ma to 359 Ma) through the latest Frasnian (385 Ma to 375 Ma). Figure 3 illustrates the generalized regional stratigraphy, after ERCB (2009).

Grosmont Formation and kartstification

The Grosmont was first described by Belyea (1952) and, despite its size, only received scant attention (Law, 1955; Norris, 1963; Belyea, 1964) until the late 1970s and early 1980s when high hydrocarbon prices motivated exploration of nonconventional reservoirs. This spurred a flurry of work by the government at the Alberta Research Council and Alberta Energy and Natural Resources (Harrison and McIntyre, 1981; Harrison, 1982, 1984, 1986; Walker, 1986; Yoon, 1986) and university scientists (Cutler, 1982; Bélanger-Davis, 1985; Hutcheon and Oldershaw, 1985; Hoffmann and Strausz, 1986; Theriault and Hutcheon, 1987; Theriault, 1988). Studies continued into the 1990s (Cotterill and Hamilton, 1995) some sponsored by AOSTRA (Luo et al., 1994; Machel and Hunter, 1994; Luo and Machel, 1995; Dembicki and Machel, 1996; Huebscher and Machel, 1997) with several corresponding related thesis available (Dembicki, 1994; Huebscher, 1996). The increased value for oil beginning in the past decade motivated reexamination of the resource with public-domain presentations regarding the Grosmont Foundation (Hein 2006; Buschkuehle et al., 2007; Hein et al., 2008; Wo et al., 2010) with academic contributions (Zhao, 2009; Borrero and Machel, 2010).

According to Borrero and Machel (2010), the Grosmont Formation is a complex of carbonate layers divided by three shale breaks representing Upper Devonian rapid deposition of substantial amounts of carbonates and basin-filling shale. Currently, the Grosmont Formation is further divided into four distinctive units on the basis of signatures in the natural gamma-ray log: the Lower Grosmont and the Upper Grosmont 1, 2, and 3 (Cutler, 1982; Harrison, 1982), which will here be called A, B, C, and D, respectively, in accordance with ERCB (2009) nomenclature. Figure 4 shows how these four units are distinguishable on the well logs from a borehole (well-02) in the study area (see the well location in Figure 5). These units are composed primarily of limestone and dolostone. Units A and B are generally of lower porosity (Hopkins and Jones, 2009; Barrett and Hopkins, 2010) than are the uppermost C and D. This difference in porosity derived from extensive kartstification. According to Huebscher (1996), kartstification occurred during the Upper Jurassic and Lower Cretaceous due to the exposure and dissolution by meteoric water. These karst features can be recognized at many scales from core samples, well logs, and high-resolution seismic data.

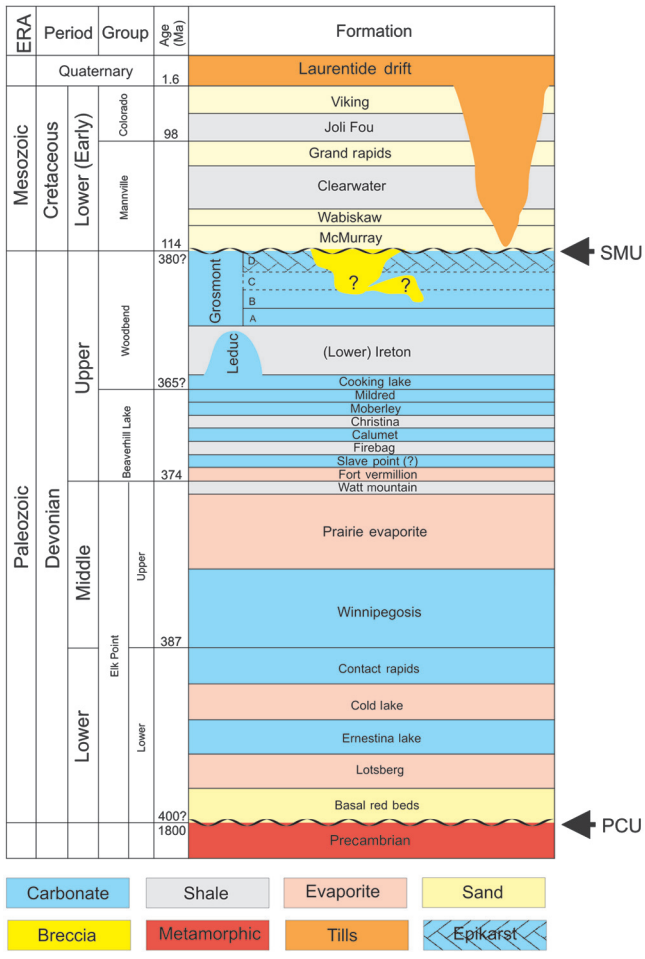

Figure 3. Generalized regional stratigraphy after ERCB (2009) and highlighting the SMU and the PCU represented as wavy lines on the stratigraphy chart.

DATA AVAILABLE AND METHODS

The obtained data sets used for this study consist of well logs and geologic formation tops, high-resolution seismic surveys, and the reported results from a vertical seismic profile (VSP). The relative location of seismic profiles, wellbores, and the VSP location is given in Figure 5. Absolute locations cannot be provided, and as such the final interpretations should be considered as an illustration of the complex geometries of the SMU. Additional details are available in Bown (2011).

Well logs and formation top data

The database accessible to us provided 99 logs and 136 geologic formation tops from 31 wells in the study area. Among the well logs, caliper, density, gamma-ray, and sonic logs are the most important wireline logs for detecting karst features (Dembicki, 1994; Dembicki and Machel, 1996; Huebscher and Machel, 1997; Machel et al., 2012). Also, sonic and density logs are required for calculation of synthetic seismograms used in the well-tie procedure. Unfortunately, most of the wells in the area just touch the SMU because they were drilled for shallow gas production; this reduced the number of logs available to reveal deeper structure within the Grosmont Formation.

Well-03 is drilled into a karst feature, and its logs provide an example of the expected responses (Figure 6). All the logs in Figure 6 are imaged in subsea true vertical depth (SSTVD). The resistivity logs in the first panel consist of invaded formation resistivity filtered at 8 inches (RXO8) and true formation resistivity (RT). RXO8 is the measurement of the flushed zone resistivity, and RT is related to the resistivity of the undisturbed formation (i.e., several meters into the formation from the borehole). In the second panel, Caliper (CAL) and environmentally corrected gamma-ray (ECGR) logs are shown. CAL represents the internal diameter of the borehole, and ECGR shows the intensity of natural gamma-ray radiation emitted from the formation. The high-resolution formation density (RHO8) and high-resolution enhanced thermal neutron porosity of limestone (HNPO-LIM) logs are illustrated in the last panel. RHO8 represents the density of bulk material, and HNPO is a measure of porosity of the formation in a selected lithology. Looking at the Grosmont D from the bottom to the top of the unit, all the presented logs are imaging different characteristics by getting closer to the SMU. RXO8 shows significant reduction of resistivity in the invaded zone (i.e., the presence of porous material saturated by brine), although the RT is measuring the same resistivity as it is in the lower part of the unit. The CAL presents enlargement of the wellbore diameter, and the boost of ECGR represents the existence of fine-grained material (such as shale, limestone contaminated with shale, or breccia) in the upper section of the unit compared with the lower section, which consists of coarse-grained limestone without showing any wellbore washout in CAL. The decrease of RHO8 means less dense material in the upper section of the unit, and HNPO-LIM growth is a complementary reference depicting the high-porosity zone. The

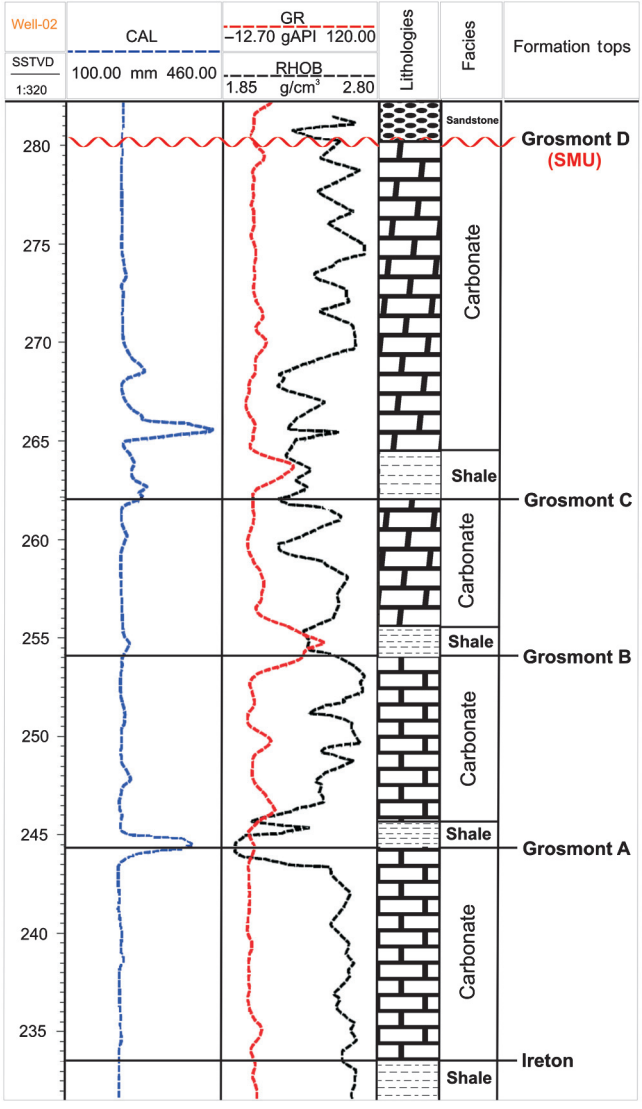

Figure 4. Well section from well-02 located southeast of the study area. Density (RHOB) and gamma-ray (GR) log signatures are used for identifying units of the Grosmont.

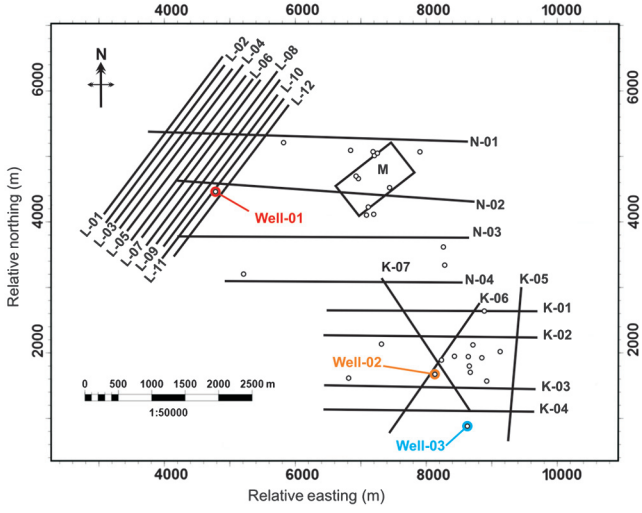

Figure 5. Map from the study area showing the approximate locations of the wellbores and seismic profiles. Exact locations cannot be provided.

Grosmont D is composed of limestone and dolostone, but as it is shown in this well section, the named logs are imaging different characteristics from the bottom of the unit to the top (SMU). These changes are all related to the karsting of the upper part of Grosmont unit D.

High-resolution seismic surveys

Four separate high-resolution seismic surveys series here called K, L, M, and N were obtained for this study (Figure 5). These high-resolution surveys at the time of acquisition in the early to mid-1980s were unique because of closely spaced receivers and sources in the later surveys. Table 1 provides a brief description of all the series acquisition parameters. Here, we review the various high-resolution seismic surveys obtained for the study:

Survey series K: Seven short 3–4-km-long profiles with closer shot and receiver spacing than would have been used in standard industry practice at the time were acquired to better image the unconformity.

Survey series L: Twelve parallel profiles spaced only 110-m apart were carried out in the area in advance of potential development. This somewhat unique survey appears to have attempted pseudo-3D coverage by having the 2D profiles in close proximity to one another.

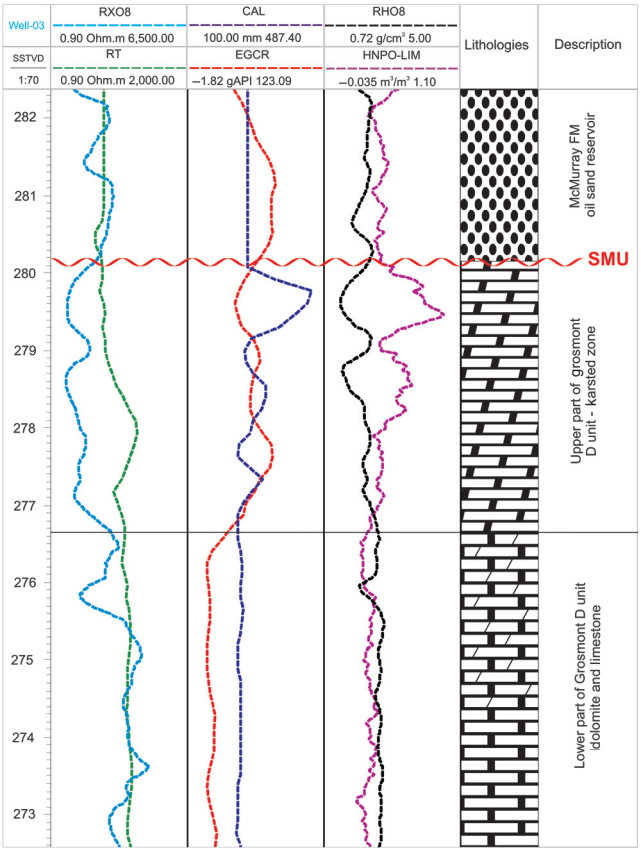

Figure 6. A well section from well-03 located southeast of the study area (see the well location in Figure 5) showing kartstification events on the right on top of Grosmont D. All the logs in this figure are imaged in SSTVD.

Table 1. Acquisition parameters deployed by the vintage seismic surveys.

Survey series	Acquisition year	Total distance	Survey type	Source	Source configuration	Source depth	Source interval	Geophone	Geophone group configuration	Group interval	Max offset	Fold	Recording parameters	Recording filters
K	1981	19.93 km	2D-Digital	Dynamite	1 × 1 kg	18 m	45 m	L-1514 Hz	6 clumped	22.5 m	540 m	12	48 traces @ 1 ms for 2 sec	Low-out High-256
L	1984	35.99 km	2D-Digital	Dynamite	1 × 0.5 kg	20 m	40 m	Mark L-28 14 Hz	12 inline over 1.8 m	10 m	480 m	12	96 traces @ 2 ms for 2 sec	Low-12 High-180
M	1985	3.21 km	3D-Digital	Pea shooter	20 drops	Surface	40 m	L-28,014 Hz	9 inline over 20 m	20 m	220 m	10	120 traces @ 2 ms for 2 sec	Low-12.5 High-125
N	1986	17.14 km	2D-Digital	Dynamite	3 × 0.1 kg	5 m	20 m	Mark OYO 14 Hz	12 inline over 10 m	10 m	250 m	12	48 traces @ 1 ms for 2 sec	Low-out High-256

Survey series M: A small full-3D seismic survey obtained over an area approximately 400 × 1000 m was an interesting experiment in seismic acquisition. The measurements were doubly unique because at the time, 3D seismic surveying was still in its infancy and had not been accepted as the primary method it is today, but also because the short source and receiver spacing used would still be rare in industrial practice. The short spacing between the sources and receivers as well as the small offsets show that its authors attempted to enhance the imaging of the unconformity surface. This was the only full survey to use a surface seismic source; all others had previously used buried dynamite. This source was called a "pea shooter" (Omnes and Robert, 1982), which is classified as a type of weight drop system in which seismic waves are generated by accelerating a mass onto a plate on the surface. Such sources have certain cost advantages in that they do not require that holes be drilled as is needed for dynamite and that they are easily moved and operated. A disadvantage of such sources, however, is that the quality of the seismic pulse put into the ground is much degraded (lower frequency and bandwidth) relative to a buried dynamite explosion. This is particularly true in marshy areas that exist at the site of the 3D survey.

Survey series N: Four high-resolution 2D profiles for survey series D were acquired to tie all of the earlier seismic lines together and fill in some of the unshot areas between them (see the profile locations in Figure 5). The acquisition parameters were developed with the results of prior experience and testing. Triple shots each of only 100 g of dynamite buried at 5-m depth provided high-bandwidth seismic energy. Nine geophones were clumped at each receiver station to increase the signal-to-noise ratio, and the stations were spaced only 10 m apart. This seismic data allow discrimination of the Grosmont C from the Grosmont D.

Seismic data processing workflows

The bulk of the efforts toward the reanalysis of these data focused first on the reprocessing of the profiles from the disparate data sets to a common elevation datum of 518 m above sea level (a.s.l.). Substantial efforts were expended in data preparation such as reformatting, organizing, editing, and merging of field geometry before the application of processing workflows. This work was also all done with an eye to the eventual integration of the disparate data sets and necessitated assigning an appropriate reference datum from which all of the reprocessing was carried out. The seismic data processing package VISTA™, provided for research purposes courtesy of GEDCO, was used for all of the data quality control and processing. The processing stream followed noise-reduction strategies in Ogunsuyi and Schmitt (2010) used for the 2D and 3D data sets and are given in Table 2. Although many of the conventional processing steps are applied, there are still specific aspects just related to the data and geologic nature of the study region.

The near-surface conditions in this area, and indeed of much of northern Alberta, are problematic to geophysical investigations due to the near-surface lateral variability. The near-surface overburden is the result of a variety of glacial and periglacial structures combined with modern-day sphagnum-moss muskeg. Glacial features can include sediment thrust faulting, creation of sub-ice-tunnel valleys that can cut as deep as the SMU, and compacted tills. Compacted tills are generally high velocity, whereas lacustrine and fluvial sediments (often coarse sands and gravels) are of lower velocity. Muskeg is problematic because it can be very low velocity (less than 600 m/s) as well as highly attenuating to the input seismic energy. This requires that careful static corrections be carried out to account for lateral varying elevations and seismic velocities. First-break picks were used to generate the velocity structure of the near surface for refraction statics corrections. Elevation statics corrections accounted for the variations in the source and

Table 2. The general sequence of 2D and 3D seismic data processing.

2D Seismic data processing sequence	3D Seismic data processing sequence
Preprocessing steps	Preprocessing steps
Geometry — load headers	Geometry — load headers
Trace editing — kill bad traces	Trace editing — kill bad traces
First-break picking	First-break picking
CMP binning	CMP binning
Elevation/refraction statics corrections	Elevation/refraction statics corrections
Fixed datum: 518 m a.s.l.	Fixed datum: 518 m a.s.l.
Refraction replacement velocity: 2255 m/s	Refraction replacement velocity: 2500 m/s
Weathering velocity: 900 m/s	Weathering velocity: 800 m/s
Scaling	Scaling
Exponential gain	Exponential gain
Surface-consistent scaling	Surface-consistent scaling
Band-pass filtering	Time-variant band-pass filtering
f-k filtering (to suppress ground roll)	Surface-consistent spiking deconvolution
Top mute	Time-variant spectrum balancing
Surface-consistent predictive deconvolution (160 ms operator length)	Iterative velocity analyses
Radial processing	Iterative residual statics corrections
Time-variant spectrum balancing	Flex binning
Iterative velocity analyses	Mute
Iterative residual statics corrections	NMO corrections and CMP stacking
Final velocity analyses	Band-pass filtering
Residual statics corrections	Automatic gain control
NMO corrections and CMP stacking	Finite difference migration
Band-pass filtering	—
Automatic gain control	—
Finite-difference migration	—

receiver elevations along the profile by positioning the data onto a common datum. Refraction statics corrections (Cox, 1999) were performed to correct the distortions associated with the variable thickness and velocity of the weathered layer.

Surface-consistent amplitude scaling was carried out to correct for the spherical divergence of the source wavefield and other attenuation effects. A top mute was carried out for the removal of the direct, refracted, and guided waves. This is essentially a brute-force removal of these strong offending arrivals from the raw shot gathers. An f-k filter was designed and applied to suppress ground roll. This worked well for survey series L and N, but it was not a suitable approach for survey series K and M because of spatially aliasing of the ground roll due to spacing. Therefore, a band-pass filter designed to reject frequencies below 20 Hz to suppress ground roll energy from series K and M data. The initial band-pass filters were applied to the individual seismic surveys as outlined in Table 3.

Predictive deconvolution was used to suppress multiples. Residual statics corrections were iteratively applied with velocity analyses. The VSP traveltimes provided reference stacking velocity trends in seismic velocity picking. The residual statics corrections are required to account for the short wavelength variations in the shallow velocity underneath each source and receiver. The surface consistent residual statics corrections were estimated by a stack power maximization algorithm.

Migration was applied to the seismic data to overcome positioning errors, collapse diffractions, and improve the vertical and lateral resolution of the images. Two migration algorithms were used: finite-difference migration (Berkhout, 1979) and Kirchhoff migration (Schneider, 1978). One example of the processed 2D profile is given for N-01 that contrasts the unmigrated stack (Figure 7a) with that corrected using Kirchhoff (Figure 7b) and finite-difference (Figure 7c) time migration. The top of the SMU is outlined in these figures just above 250 ms of the two-way traveltime. Close examination of the unmigrated profile reveals numerous small diffractions or related (bowtie) seismic arrival features. Such features are produced by geologic structures of spatial dimensions similar to the seismic wavelengths used to illuminate the subsurface. Such structures scatter seismic energy in all directions producing localized convex, hyperbolic seismic events, the apex of which marks the location of the scatterer. The complicated texture of the seismic events immediately beneath the SMU in Figure 7a is consistent with a series of small diffractions. This character differs significantly from the flatter and more continuous Mesozoic sediments above the SMU that do not display diffractions. The diffractions beneath the SMU are consistent with, but not conclusive of, a rough karsted topography with features too small to be properly imaged but which could still scatter the seismic energy. The migrated profiles in Figure 7b and 7c show better lateral continuity of the events

Table 3. List of initial band-pass filters applied to the seismic data.

Survey Series	Band-pass filter (Hz) (low truncation/low corner — high corner/high truncation)	Comments
K	17-20-190-250	Low frequencies were removed for the suppression of ground roll.
L	8-12-150-175	—
M	17-20-125-150	Low frequencies were removed for the suppression of ground roll.
N	8-12-190-250	—

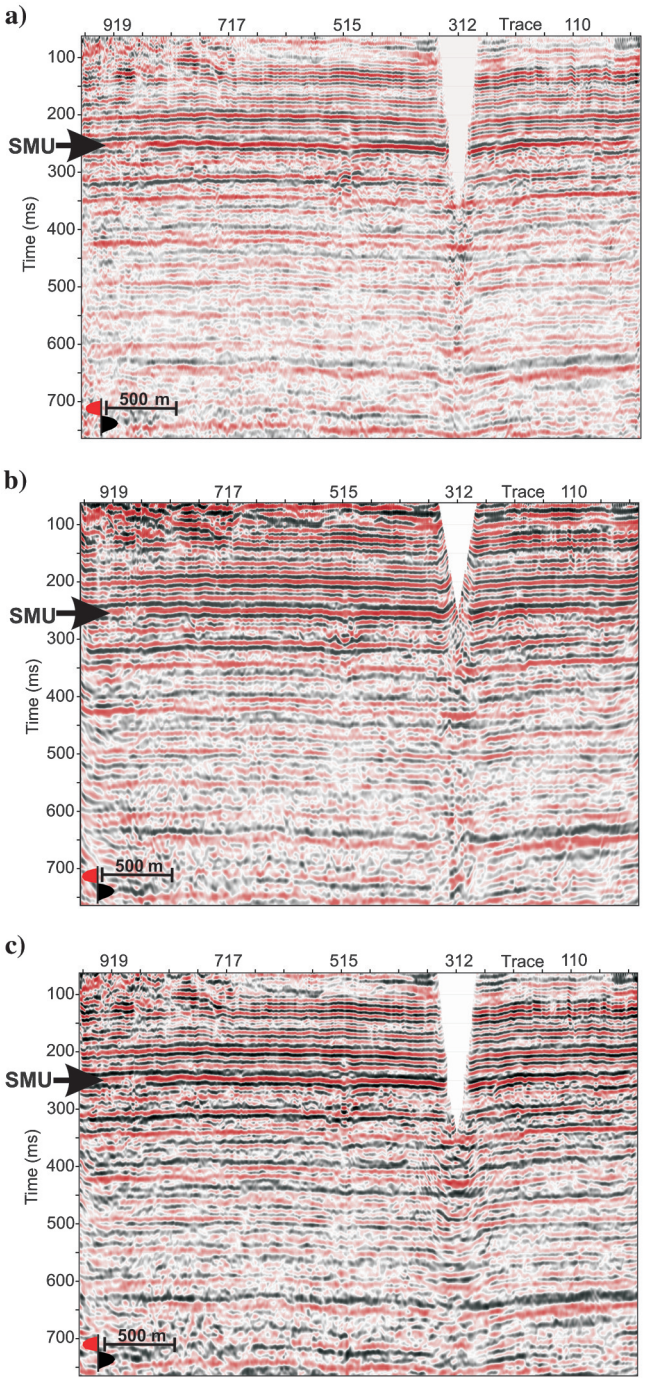

Figure 7. Examples of the final processed seismic profile 01 from the N series. Upon (a) final stack, (b) Kirchhoff-migrated profile, and (c) finite-difference migrated profile.

immediately beneath the SMU; this is completely expected because one main purpose of migration is to collapse the diffraction back to its original scattered location. This comparison reinforces the need for the best practice of using the unmigrated and the migrated data in interpretation. In the case studied here, the unmigrated data may actually provide more information on the location of scattering geologic structures.

Naturally, the processing of the 3D data differed from that for the 2D profiles but was further complicated by the low-energy weight-drop seismic source used. Such sources allow for multiple shots at each source location, but the source signature is of lower quality relative to dynamite. The processing followed procedures much like those used for the 2D data, although additional care was given to deconvolution of the data due to the poorer signal quality.

Some examples of processed seismic lines from different series are shown in Figure 8. Comparison of these profiles in Figure 8 reveals the lower data quality of the 3D profiles relative to the 2D dynamite lines. This is in part due to the low 3D bin folds, the effects of static corrections in the area, and the type of source used. Regardless, Figure 8 illustrates the progression of data quality as experience was gained during the different surveys.

INTEGRATION OF THE DATA SETS AND INTERPRETATION

A high-resolution VSP and an extensive series of well logs were obtained in well-01. The combination of this data allowed for the geology to be tied to the seismic images. Unfortunately, the original digital VSP data remains lost and could not be further processed to provide additional information on the reflectivity and multiple reflections. Only the time-to-depth time picks and an image of the raw VSP data are still available (Figure 9). This imaged VSP data provided constraints on seismic traveltimes that were important in assisting with the processing of the seismic data and in the interpretation of the profiles. The one-way traveltime of the VSP (blue diamonds) is plotted with the gamma-ray log (green line) of the well for the interpretation of the individual Grosmont members. According to this comparison, the SMU resides at a true vertical depth of 250 m, which corresponds to a two-way seismic traveltime of about 240 ms. Sonic and density logs were acquired over a limited depth range from 180 to 400 m and used to generate a synthetic trace (Figure 10) based on a wavelet extracted from the nearby seismic traces. In this synthetic, the strong positive peak at 242 ms is associated with the SMU. Despite the limitations of the VSP and well-log data, the four different seismic surveys of K, L, M, and N could be integrated by the prominent SMU horizon because in all of these data sets, the most prominent event is related to the SMU. It should be noted that the polarity of the N-series profiles was reversed probably during the original acquisition of the data but it was apparent at tie points and easily corrected. The strong event at the SMU is not unexpected given the large impedance contrasts between the Devonian carbonates and the Cretaceous siliciclastic rocks.

The VSP data were also used to develop an appropriate time to depth velocity model that allowed for conversion of the observed traveltimes into true elevations. The model is summarized in Table 4, with Figure 11 showing how the model varies in space over the Grosmont surface. Although this model is variant over the Wabiskaw-SMU and SMU-Ireton zones, the constant velocity has been used for rest of the zones due to the lack of geologic tops deeper than Ireton for obtaining velocity surfaces. These constant velocities were computed using VSP for each individual zone.

A few prominent seismic reflection horizons have been selected for interpretation, and these are assigned to the various geologic tops on the seismic profiles. However, the general lack of appropriate logs as well as the paucity of boreholes penetrating deeper than the Grosmont complicates this interpretation. The VSP data were critical to obtaining approximate lithological ties above the SMU horizon, and lithologies deeper in the seismic section were confirmed by comparison to the interpreted regional geology knowledge. Figure 12 shows these events on the profile L-11 with the synthetic seismogram used for the well tie. The seismic events used for mapping and further interpretation are associated with the

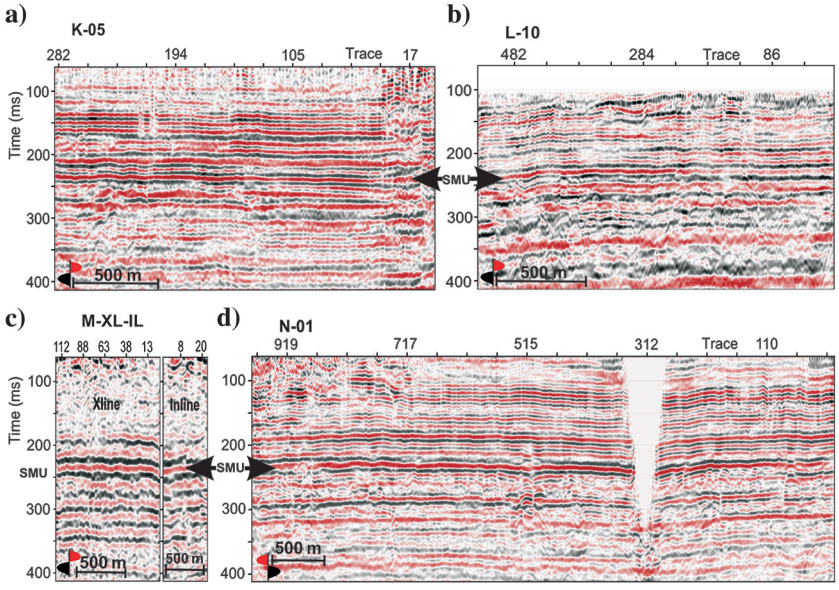

Figure 8. Some examples of processed seismic profiles from different seismic series showing data quality evolution from the first survey to the latest. Upon (a) profile 05 from the K series, (b) profile 10 from the L series, (c) crossline and inline profiles from the M series, and (d) profile 01 from the N-series.

geologic formations of the Clearwater, the Wabiskaw, the Grosmont (SMU), the Lower Ireton, the Prairie Evaporate, and finally, the Pre-Cambrian crystalline basement (PCU). Once the traveltimes to these various horizons are picked, they may be turned into maps of the surfaces in terms of seismic time, depth surfaces calculated using an appropriate velocity model, and isopach surfaces that reveal the variations in thicknesses of the intervals between two reference layers.

Figure 13 shows three different views of the SMU (top Grosmont D) surface elevation as determined solely from the sparse stratigraphic tops from well logs (Figure 13a), the reflection times directly picked from the integrated seismic profiles (Figure 13b), and the time-to-depth converted SMU elevations (Figure 13c). In these plots, the surfaces were interpolated using the convergent gridding method. This algorithm uses a coarse grid, which is

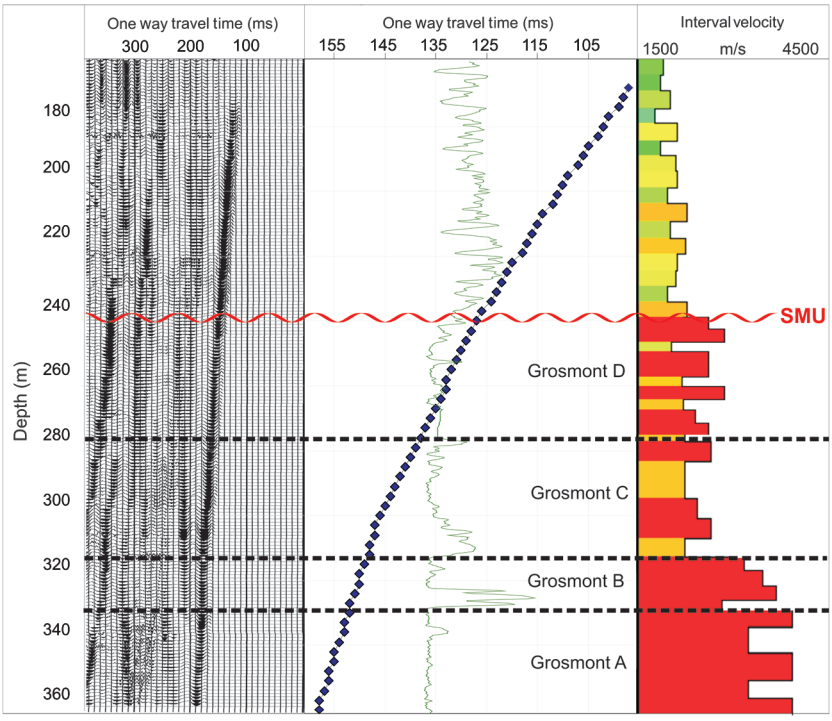

Figure 9. The left panel shows the image of the VSP from a confidential pilot project report for well location W-01. The middle panel shows the one-way traveltime of the VSP data (blue diamonds) superimposed on the unscaled gamma log. The interval velocity calculated using VSP data is illustrated in the right panel. The red color indicates the higher interval velocities.

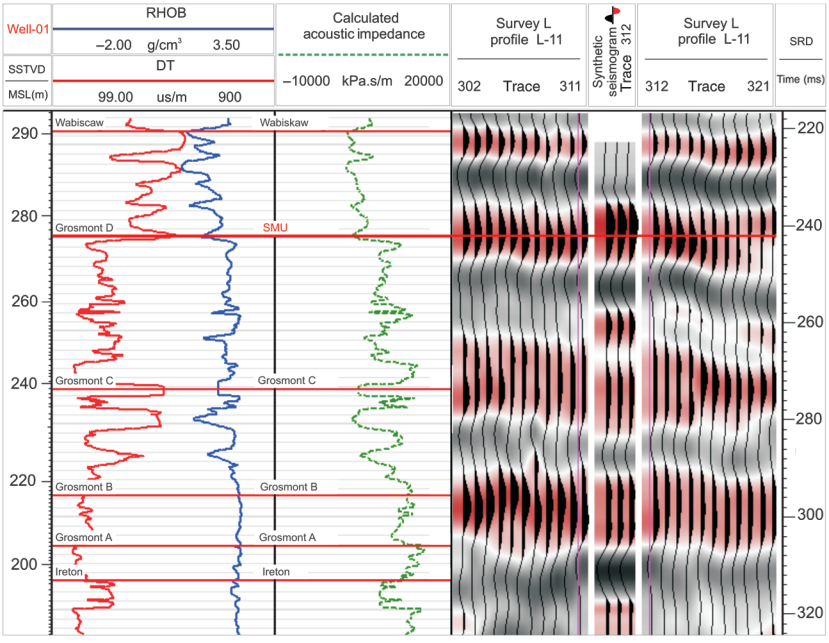

Figure 10. The correlation of a portion of seismic profile L-11 and constructed synthetic seismogram with the well logs used to generate a synthetic trace at the location of well-01. The calculated acoustic impedance and reflection coefficient are illustrated in the middle panels.

initially assigned to the data and then refined many times until the surface converges to a specified smoothness. The convergent gridding is a fast and general-purpose extrapolation algorithm for randomly distributed scatter data points. It adapts to sparse or dense distribution through converging iterations at successively finer grid resolutions.

The well elevation map (Figure 13a) has 17 wells that reach the SMU, but their positions were highly biased to the actual pilot project sites. In comparison, the seismic data show substantially more detail. Chiefly, the SMU varies on a smaller scale than the overall spatial sampling of well data; thus, the well elevation map fails to adequately capture the topography of the SMU. Further, the validity of some of the well tops could not be confirmed because the original log data were not available for quality-control purposes in some of the boreholes. Therefore, the final interpretation was conducted only on time elevation surfaces. Looking at Figure 13b, the time difference from the highest to the lowest point of the map is 32 ms in two-way traveltime. This suggests that topographic variations are on the order of 35 m. Whether the actual variations are that large could be questioned, but the seismic data and the resulting map provide strong evidence for the rapidly varying topographic features.

At this point, it is important to question the resolving power of the seismic data. One rule of thumb for the resolving capability is given by the Rayleigh one-quarter wavelength, or the first Fresnel zone, criterion with radius R given by

$$R = \frac{V}{2}\sqrt{\frac{t}{f}} = \sqrt{\frac{Z\lambda}{2}}, \tag{1}$$

where V is the seismic velocity overlying the structure, t is the two-way traveltime, f is the frequency, Z is the depth, and λ is

Table 4. Summary of the velocity model used to convert two-way traveltimes to elevations.

Top surface	Bottom surface	Velocity model	Comments
Seismic reference datum: 518 m a.s.l.	Ground surface	Constant interval velocity: 1720 m/s	Replacement velocity
Ground surface	Clearwater	Constant interval velocity: 2200 m/s	Determined from VSP
Clearwater	Wabiskaw	Time to depth relation	Velocity surface made from check shots
Wabiskaw	Grosmont D (SMU)	Time to depth relation	Velocity surface made from check shots
Grosmont D (SMU)	Ireton	Time to depth relation	Velocity surface made from check shots
Ireton	Prairie evaporite	Constant interval velocity: 4900 m/s	Determined from VSP
Prairie evaporite	Pre-Cambrian Basement	Constant interval velocity: 5400 m/s	No data — reasonable estimate
Pre-Cambrian Basement (PCU)	—	Constant interval velocity: 6000 m/s	No data — reasonable estimate

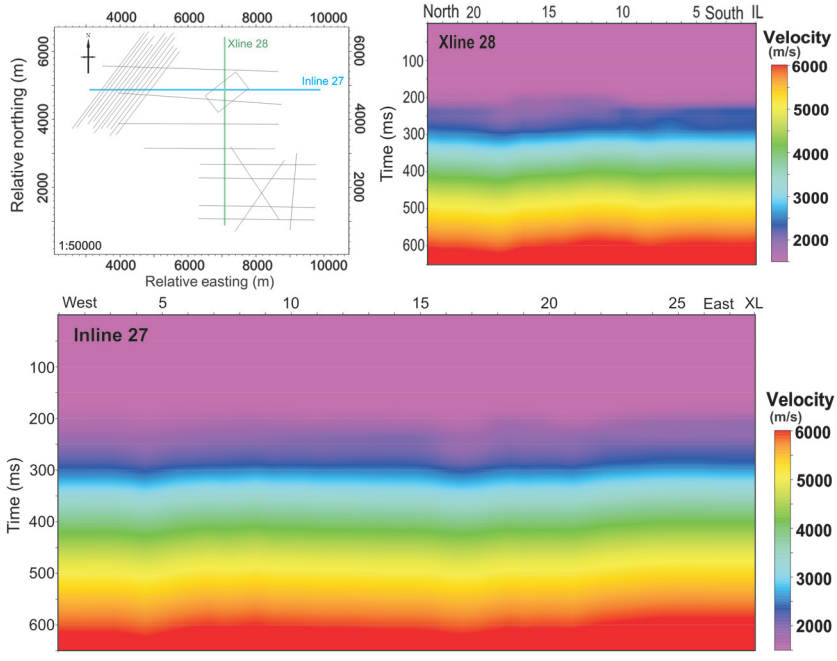

Figure 11. Displaying inline and crossline profiles of the generated velocity model used for depth conversion.

the wavelength. Using representative numbers of V (2500 m/s), t (250 ms), and f (50 Hz) suggests that the radius of the Fresnel zone is more than 80 m. Migration of the seismic data may halve that number, but this still means that resolving features less than 40 m is difficult with these legacy profiles. As such, the current data set can only confidently image the larger topography of the SMU. It cannot detect rapid variations in the topography that might be caused at the edge of a sinkhole nor could it adequately resolve a sharp cliff.

The SMU time surface of Figure 14 is reproduced at a larger scale. There are two primary east–west trends observed in this image, ridge A and a valley B. The valley and ridge were measured up to a kilometer width. Feature C appears to be a small linear valley running in a northeast–southwest alignment. Strong evidence of this narrow valley was observed in line N-01 running nearly perpendicular to this structure. The response of this narrow karst valley is clearly seen on the seismic section displayed Figure 15 by a shift later in two-way traveltime of the SMU. The valley was estimated to be about 330-m wide (270 m if normal to the strike of the valley). Further analyzing the valley, one can observe a secondary feature of what appears to be about a 50-m-wide channel equivalent to a 35 m normal to the strike of the valley (Figure 15) possibly cut into the bottom of the valley. Moreover, this northeast–southwest orientation of feature C may be subparallel to the expected joint trends in the Grosmont Formation (Jones, 2010). Evidence for this feature was support on the ties between the series L and series N data sets.

A comparison of surface structure of SMU against the other five interpreted time surfaces is shown in Figure 16 in sequential order from shallow to deep. The Mesozoic Clearwater (Figure 16a) and the Wabiskaw (Figure 16b) surfaces correlate with the SMU (Figure 16c). This suggests that the sedimentation above the SMU was influenced by its topography. The reasons for this are not known but could be indicative of collapse of the karsted SMU, differential compaction of the Mesozoic sediments, or even fault motions.

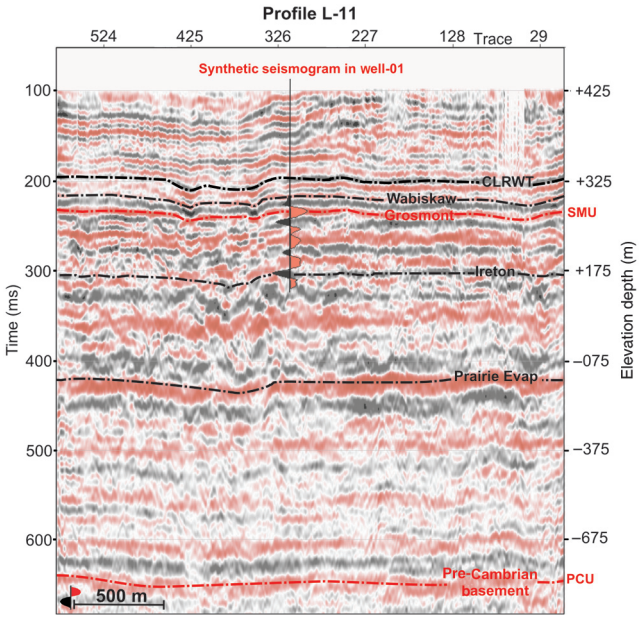

Figure 12. The synthetic seismogram plotted on the seismic profile L-11 at well-01. Example time picks for the seismic horizons selected for mapping are shown by the dotted-dashed line.

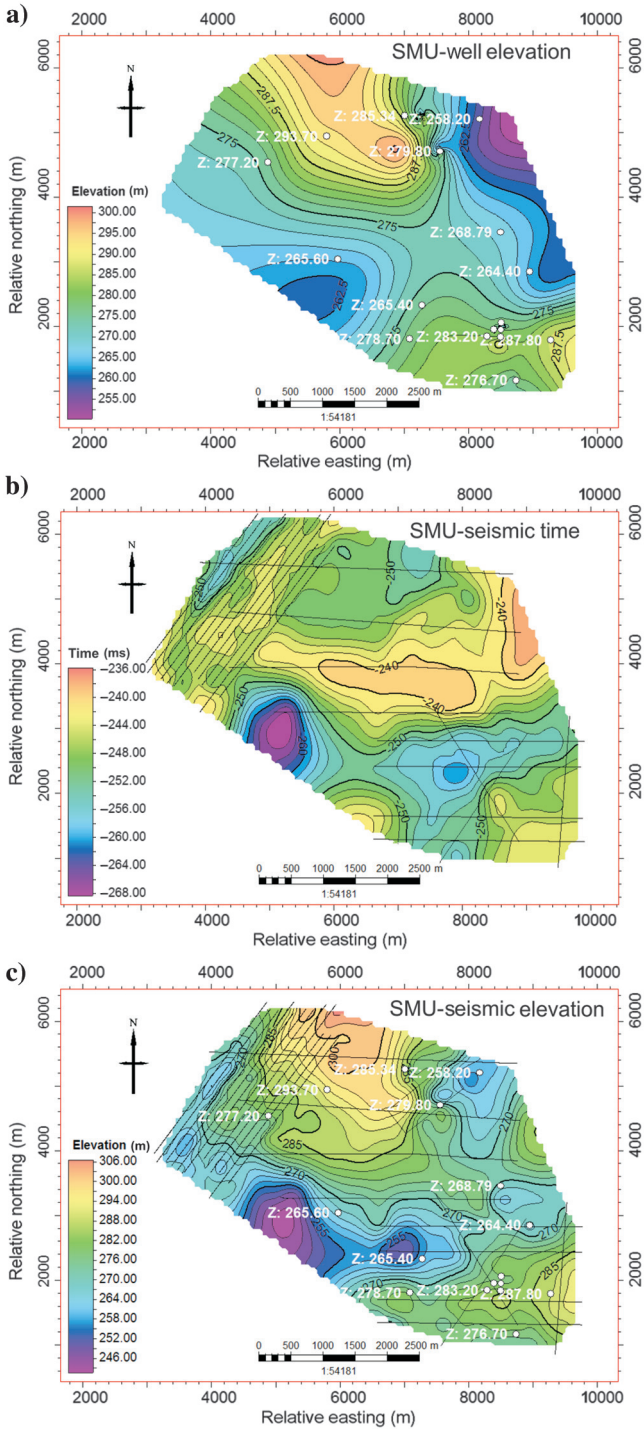

Figure 13. Comparison of the surface maps for the SMU as determined from interpolation of (a) well-log top information, (b) the picked seismic times from the legacy seismic data processed in this study, and (c) the seismic elevations as estimated from (b) using the velocity model. The location of the wells and seismic lines and well markers elevation depth is posted on these maps.

Despite the poor imaging of our seismic data at later times of the profiles, lateral disturbances in the continuity of the seismic reflectors can be observed. These features are particularly more obvious in the profiles trending southeast–northwest and southwest–northeast. Seismic profile K-7 (Figure 17a) shows such a disturbance zone. According to Kellett et al. (1994, 2005), the presence of strong diffractions extending to depth, cone-shaped disturbances, and apparent pull-up and pull-down in different parts of the seismic section may be indicative of igneous intrusives. Evidence for the existence of such features in the study area comes from the filtered high-resolution aeromagnetic (HRAM) data, which show magnetic lineaments (Figure 17b) that are possibly interpreted as igneous dykes. We cannot as yet confirm these as dykes due to a lack of appropriate geologic information. Best (1988) and Airo and Wennerström (2010) see similar features in the region immediately to the northeast of this study that they interpret to be faults in the sediments and within the metamorphic basement.

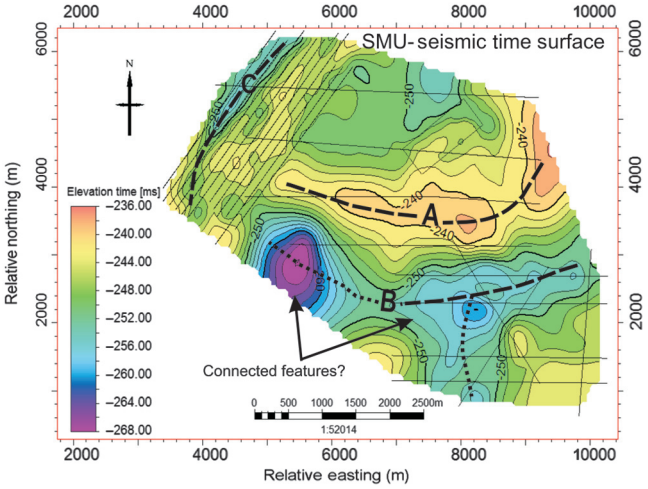

Figure 14. Expanded scale of Figure 12b for the picked seismic time surface for the SMU. Curved lines A and B highlight the axes of a detected ridge and a valley running roughly east–west across the study area. Axis C highlights the location of a smaller, less certain, valley running in a northeast–southwest direction.

The observed lineaments, regardless of their interpretation as either igneous dykes or faults, can have a significant role in the karstification of the Grosmont Formation. When dykes propagate vertically upward through the sediment overburden, hot volatiles and gases would escape above the dike tip (Wall et al., 2010). The escaped fluids may induce fractures, depression, and dissolution of the overlaid Upper Elk point, Beaverhill Lake, and Woodbend sedimentary groups. Faults also can act as preferential zones of enhanced fluid (surface or underground water) flow. That said, we must always be cautious about seismic processing artifacts. Vertical and subvertical artifacts can be produced by the existence of the low seismic velocity region, surrounded with higher seismic velocity strata. Reprocessing and examination of the near and far seismic data would result in a better understanding of these kinds of features.

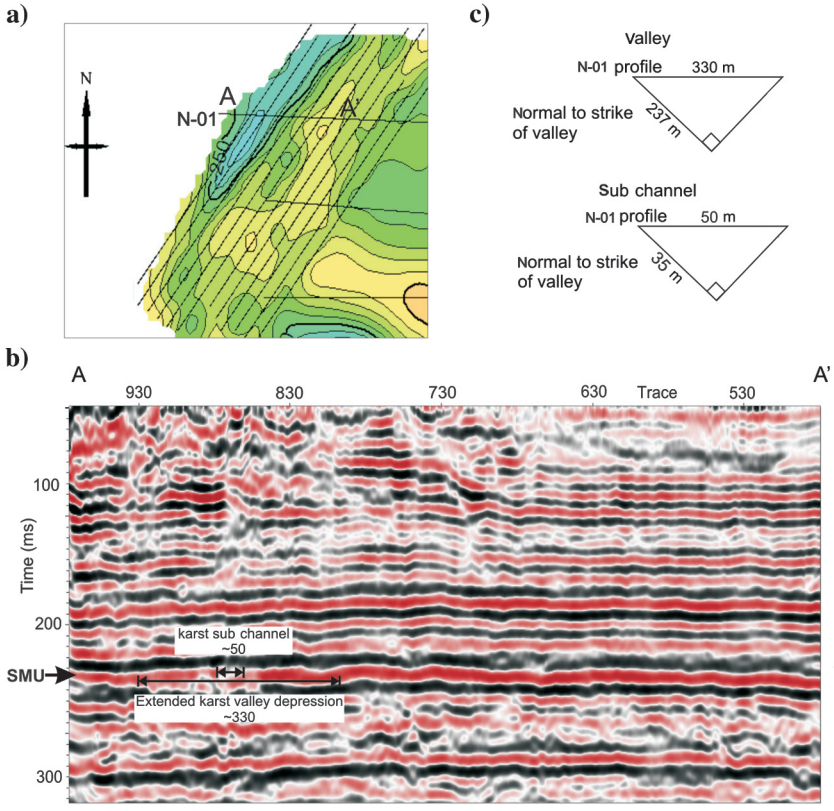

Figure 15. Feature C, an imaged karst valley in the seismic data of (a) the time map of the SMU, (b) a portion of seismic line N-01 profiling A-A′, and (c) the geometry of the apparent width and the true width of karst valley and subchannel.

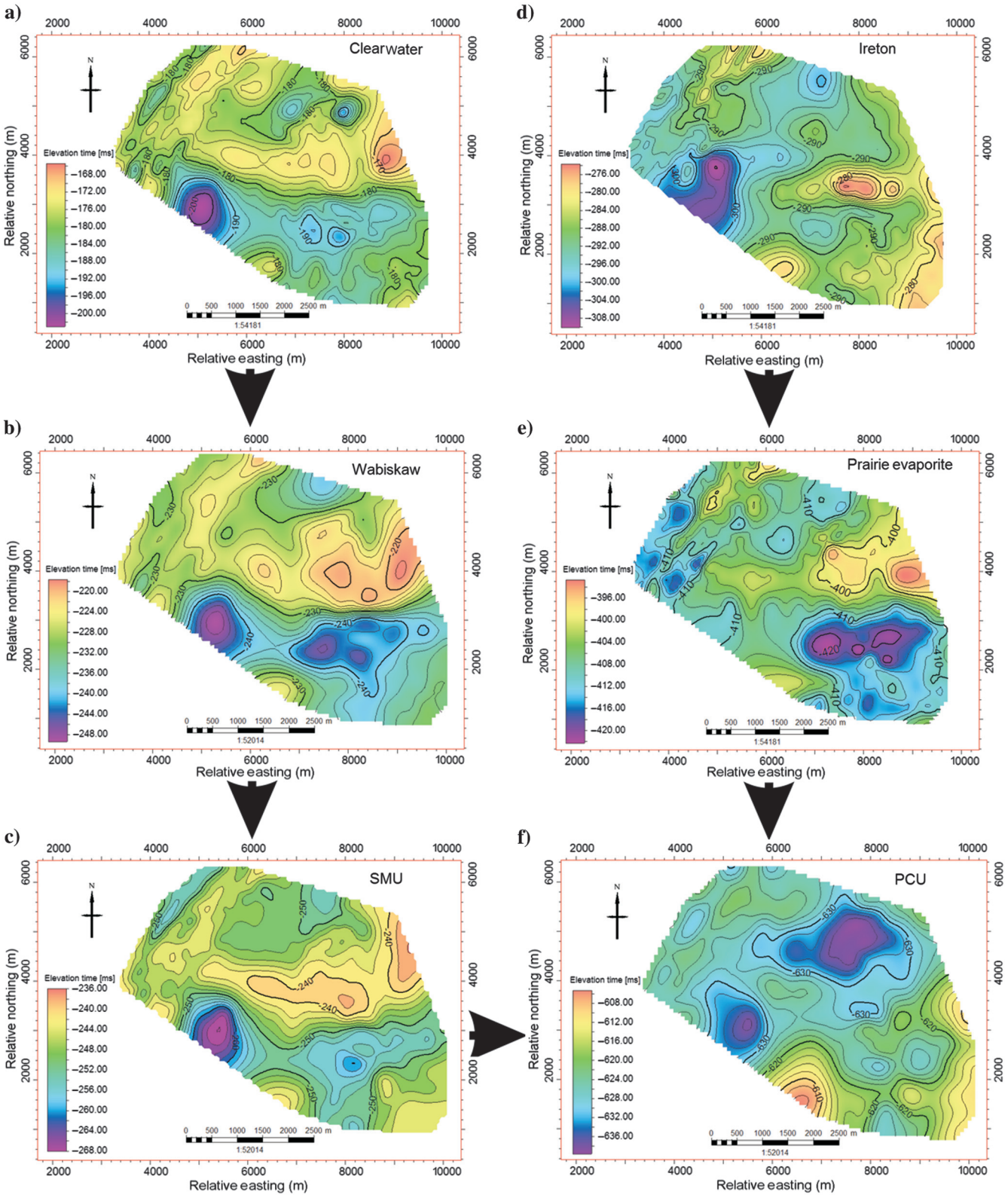

Figure 16. Comparison of the surface maps in time domain for the (a) Mesozoic Clearwater, (b) Mesozoic Wabiskaw, (c) SMU, (d) Paleozoic Ireton, (e) Paleozoic Prairie Evaporite, and (f) PCU. Arrows denote the progression of the panels with subsequently increasing depth.

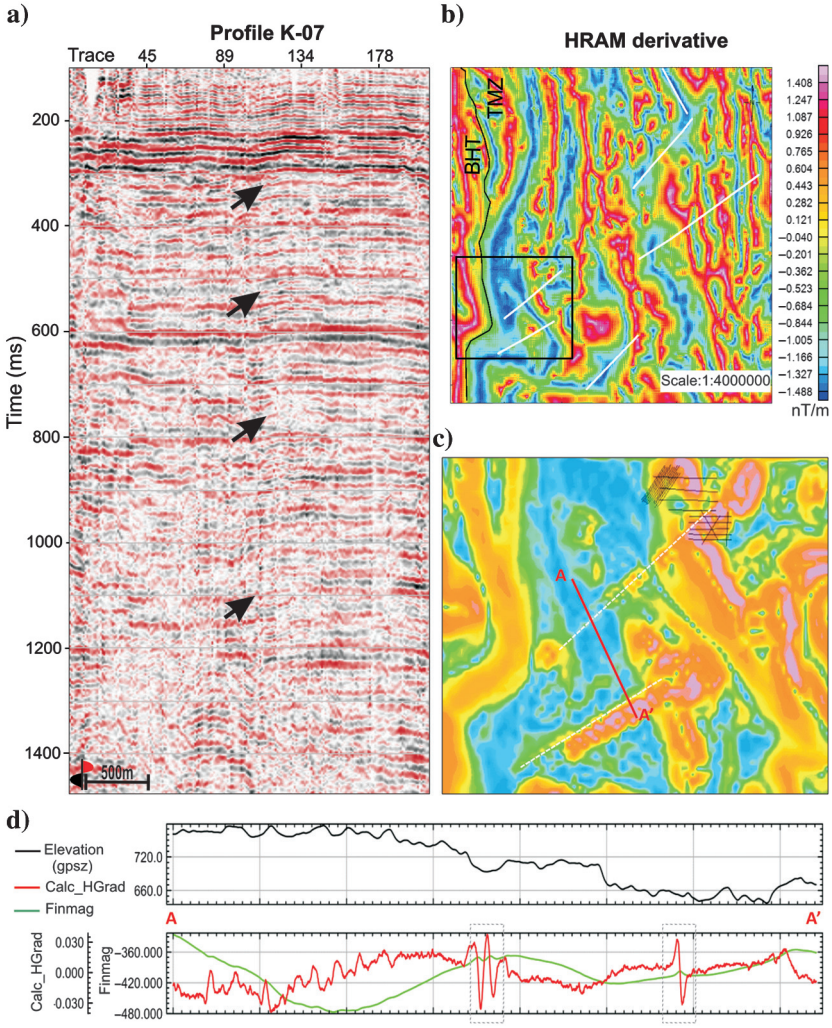

Figure 17. Illustration of the possible structures in the study area: (a) seismic disturbance zone on seismic profile K-07, (b) tilt derivative of magnetic anomaly map with the suggested lineaments and boundary of the Taltson Magnetic Zone and Buffalo Head Terrane, (c) the magnified filtered magnetic image over the seismic surveys showing the lineament crossing the area (seen on the seismic profile K-01). (d) Profile A-A′ is almost perpendicular to the lineaments of interest. This profile is depicted at the lowermost part of the picture; black, green, and red graphs, respectively, represent elevation (gpsz), reduced to the pole residual magnetic, and (Finmag) and calculated horizontal derivative of the residual magnetic (Calc_HGrad). The black rectangles highlight magnetic lineaments in the area of interest.

CONCLUSION

The interpreted time structure maps of the Grosmont (SMU) and the overlying and underlying formation tops show substantially more detail than those constructed on the basis of well-log information only; in fact, the use of only well-log information would likely result in erroneous interpretations. Although features smaller than about 40 m in radius could not be easily discerned at the SMU due to wavefield and data sampling limits, the data do reveal the existence of a ridge-valley pattern. The model such as we describe here may occur in any basin that has a deep, relatively thick section of Paleozoic carbonates that underlie major unconformities. Comparison of the structural maps from surfaces below the SMU suggests that deeper features (intrusion bodies/faults) may also influence the structure of the SMU. HRAM data in the study area confirm the existence of such deeper features. Meanwhile, the overlying Mesozoic formations represent almost the same structural topography as the SMU surface. This may be due to the collapse of karst features within the Grosmont after Mesozoic deposition, differential compaction of the Mesozoic sediments, or even small fault motions. The current reexamination and integration of the legacy project data sets demonstrate the necessity for geophysical studies of this resource. Additional work would assist in adding value to any modern seismic data obtained in the production of this resource.

ACKNOWLEDGMENTS

F. Ogunsuyi and A. Oncel assisted in the analysis of these data. S. Kotkas, R. Sawatsky, and C. Tunney expedited locating and obtaining the legacy seismic profiles; these results are rehearsed from Bown (2011). The magnetic data are provided under purchased license from Stornoway Diamonds as assisted by B. Charters and J. Peirce. The initial components of this study were supported within the Carbonates Research Program of the Alberta Research Council (now Alberta Innovates–Technology Futures). Access to the magnetic data in the area as well as support for E. P. Ardakani were granted by the geothermal exploration theme of the Helmholtz Alberta Initiative.

REFERENCES

Airo, M. L., and M. Wennerström, 2010, Application of regional aeromagnetic data in targeting detailed fracture zones: Journal of Applied Geophysics, **71**, 62–70, doi: 10.1016/j.jappgeo.2010.03.003.

Barrett, K. R., and J. C. Hopkins, 2010, Stratiform carbonate breccias of the Grosmont Formation, Alberta: Presented at AAPG 2010 International Conference and Exhibition.

Bélanger-Davis, C. E., 1985, Mineralogical and petrophysical changes after steam testing in carbonate rocks of the Grosmont Formation, Alberta: M.S. thesis, University of Calgary.

Belyea, H. R., 1952, Notes on the Devonian system for the north-central plains of Alberta: Geological Survey of Canada.

Belyea, H. R., 1956, Grosmont Formation in the Loon Lake area: Petroleum Geology, **4**, 66–69.

Belyea, H. R., 1964, Upper Devonian, Part II — Woodbend, Winterburn and Wabamun Groups, *in* R. G. McCrossan, and R. P. Glaister, eds., Geological history of Western Canada: Alberta Society of Petroleum Geologists, 66–68.

Berkhout, A. J., 1979, Steep dip finite-difference migration: Geophysical Prospecting, **27**, 196–213, doi: 10.1111/j.1365-2478.1979.tb00965.x.

Best, M. G., 1988, Early Miocene change in direction of least principal stress, southwestern United States; Conflicting inferences from dikes and metamorphic core-detachment fault terranes: Tectonics, **7**, 249–259, doi: 10.1029/TC007i002p00249.

Borrero, M. L., and H. G. Machel, 2010, Sedimentology and diagenesis of Hondo Evaporites within the Grosmont giant heavy oil carbonate reservoir, Alberta, Canada: Presented at AAPG 2010 International Conference & Exhibition.

Bown, T. D., 2011, Legacy seismic investigations of karst surfaces; implications for heavy oil extraction from the Devonian Grosmont Formation, northeastern Alberta, Canada: M.S. thesis, University of Alberta.
Buschkuehle, B. E., F. J. Hein, and M. Grobe, 2007, An overview of the geology of the Upper Devonian Grosmont carbonate bitumen deposit, northern Alberta, Canada: Natural Resources Research, **16**, 3–15, doi: 10.1007/s11053-007-9032-y.
Cotterill, D., and W. N. Hamilton, 1995, Geology of Devonian limestones in northeast Alberta: Alberta Geology Survey, Open file report, 1995-07.
Cox, M. J. G., 1999, Static corrections for seismic reflection surveys: SEG.
Cutler, W., 1982, Stratigraphy and sedimentology of the Upper Devonian Grosmont Formation, Alberta, Canada: M.S. thesis, University of Calgary.
Dembicki, E. A., 1994, The Upper Devonian Grosmont Formation; well log evaluation and regional mapping of a heavy oil carbonate reservoir in northeastern Alberta: M.S. thesis, University of Alberta.
Dembicki, E. A., and H. G. Machel, 1996, Recognition and delineation of paleokarst zones by the use of wireline logs in the bitumen-saturated Upper Devonian Grosmont Formation of northeastern Alberta, Canada: AAPG Bulletin, **80**, 695–712.
Energy Resources Conservation Board, 2009, Table of formations, http://www.ercb.ca/docs/products/catalog/TOF.pdf, accessed 27 July 2012.
Energy Resources Conservation Board, 2010, Alberta's energy reserves 2009 and supply/demand outlook 2010–2019, Open file report ST98-2010.
Harrison, R., 1982, Geology and production history of the Grosmont carbonates pilot project, Alberta, Canada: Presented at Second United Nations Institute for Training and Research Conference on Future of Heavy Crude and Tar Sands.
Harrison, R., 1984, The bitumen-bearing Paleozoic carbonate trends of northern Alberta: Presented at AAPG 1984 Research Conference.
Harrison, R., 1986, Regional geology and resource characterization of the Upper Devonian Grosmont Formation, northern Alberta: Alberta Research Council.
Harrison, R., and B. McIntyre, 1981, The geologic setting of the Grosmont thermal recovery project, northeastern Alberta: Presented at Alberta Oil Sands Technology and Research Authority (AOSTRA) Seminar on Advances in Petroleum Upgrading and Recovery Technology.
Hein, F. J., 2006, Heavy oil and oil (tar) sands in north America: An overview and summary of contributions: Natural Resources Research, **15**, 67–84, doi: 10.1007/s11053-006-9016-3.
Hein, F. J., R. Marsh, and M. Boddy, 2008, Overview of the oil sands and carbonate bitumen of Alberta: Regional geologic framework and influence of salt-dissolution effects: Presented at AAPG Hedberg Conference.
Hoffmann, C. F., and O. P. Strausz, 1986, Bitumen accumulation in Grosmont platform complex, Upper Devonian, Alberta, Canada: AAPG Bulletin, **70**, 1113–1128.
Hopkins, J., and B. Jones, 2009, Reservoir units in the Grosmont Formation: Stratigraphy, paleotopography and reservoir geology of the Grosmont Formation Twp 80-90 Rge 12-21W4: Alberta Research Council and Carbonate Research Program, Geology report 0708-1.
Huebscher, H., 1996, Regional controls on stratigraphic and diagenetic evolution of the Woodbend group carbonates, north central Alberta, Canada: M.S. thesis, University of Alberta.
Huebscher, H., and H. G. Machel, 1997, Paleokarst in the Grosmont Formation, northeastern Alberta, *in* J. Wood, and B. Martindale, eds., Core Conference: Canadian Society of Petroleum Geologists for Sedimentary Geology Joint Convention, CSPG-SEPM, 129–151.
Hutcheon, I., and A. Oldershaw, 1985, The effect of hydrothermal reactions on the petrophysical properties of carbonate rocks: Bulletin of Canadian Petroleum Geology, **33**, 359–377.
Jones, B., 2010, Fracture systems in the Grosmont Formation: Alberta Research Council and Carbonate Research Program Geology, Report 0910-8a.
Kellett, R. L., A. E. Barnes, and M. Rive, 1994, The deep structure of the Grenville Front; a new perspective from western Quebec: Canadian Journal of Earth Sciences, **31**, 282–292, doi: 10.1139/e94-027.
Kellett, R. L., G. J. Steensma, and R. M. Zahynacz, 2005, Geophysical signature of the Mountain Lake intrusion; a study to support future kimberlite exploration in Alberta: Alberta Geological Survey and Alberta Energy and Utilities Board, Special report 064.
Law, J., 1955, Geology of northwestern Alberta and adjacent areas: AAPG Bulletin, **39**, 1927–1978, doi: 10.1306/5CEAE29E-16BB-11D7-8645000102C1865D.
Luo, P., and H. G. Machel, 1995, Pore-size and pore throat types in a heterogeneous dolostone reservoir, Devonian Grosmont Formation, Western Canada sedimentary basin: AAPG Bulletin, **79**, 1698–1720.
Luo, P., H. G. Machel, and J. Shaw, 1994, Petrophysical properties of matrix blocks of a heterogeneous dolostone reservoir — The Upper Devonian Grosmont Formation, Alberta, Canada: Bulletin of Canadian Petroleum Geology, **42**, 465–481.
Machel, H. G., 2010, The Devonian petroleum system of the Western Canada Sedimentary Basin with implications for heavy oil reservoir geology, *in* S. Chopra, L. R. Lines, D. R. Schmitt, and M. L. Batzle, eds., Heavy oils: Reservoir characterization and production monitoring: SEG, Geophysical Developments Series, no. 13, 131–154.
Machel, H. G., M. L. Borrero, E. Dembicki, H. Huebscher, P. Luo, and Y. Zhao, 2012, The Grosmont: The world's largest unconventional oil reservoir hosted in carbonate rocks, *in* J. Garland, J. E. Neilson, S. E. Laubach, and K. J. Whidden, eds., Advances in carbonate exploration and reservoir analysis: Geological Society of London, Special Publication, 370, 49–81.
Machel, H. G., and I. Hunter, 1994, Facies models for middle to late Devonian shallow marine carbonates, with comparisons to modern reefs: A guide for facies analysis: Facies, **30**, 155–176, doi: 10.1007/BF02536895.
Mossop, G., and I. Shetsen, 1994, Geological atlas of the Western Canada Sedimentary Basin: Canadian Society of Petroleum Geologists and Alberta Research Council.
NASA, 2012, MODIS, http://modis.gsfc.nasa.gov, accessed 10 July 2012.
Norris, A., 1963, Devonian stratigraphy of northeastern Alberta and northwestern Saskatchewan: Geological Survey of Canada, Memoir 313.
Ogunsuyi, F., and D. R. Schmitt, 2010, Integrating seismic velocity tomograms and seismic imaging: Application to the study of a buried valley, *in* R. D. Miller, J. D. Bradford, and K. Holliger, eds., Near surface seismology and ground penetrating radar: SEG, 361–378.
Omnes, G., and P. Robert, 1982, The P-Shooter1: A fast seismic source for shallow exploration: Geophysics: AAPG Bulletin, **66**, 1697.
Schneider, W. A., 1978, Integral formulation for migration in two and three dimensions: Geophysics, **43**, 49–76, doi: 10.1190/1.1440828.
Switzer, S. B., W. G. Holland, D. S. Christie, G. C. Graf, A. S. Hedinger, R. J. McAuley, R. A. Wierzbicki, and J. J. Packard, 1994, Devonian Woodbend-Winterburn strata of the western Canada sedimentary basin, *in* G. D. Mossop, and I. Shetsen, eds., Geological Atlas of the Western Canadian Sedimentary Basin: Canadian Society of Petroleum Geologists and Alberta Research Council.
Theriault, F., 1988, Lithofacies, diagenesis, and related reservoir properties of the Upper Devonian Grosmont Formation, northern Alberta: Bulletin of Canadian Petroleum Geology, **36**, 52–69.
Theriault, F., and I. Hutcheon, 1987, Dolomitization and calcitization of the Devonian Grosmont Formation, northern Alberta: Journal of Sedimentary Petrology, **57**, 955–966, doi: 10.1306/212F8CB5-2B24-11D7-8648000102C1865D.
Walker, D., 1986, Regional stratigraphy of the Upper Devonian Grosmont Formation, northern Alberta: Alberta Geological Survey, open file report, 1986-02.
Wall, M., J. Cartwright, R. Davies, and A. McGrandle, 2010, 3D seismic imaging of a Tertiary Dyke Swarm in the southern North Sea, UK: Basin Research, **22**, 181–194, doi: 10.1111/j.1365-2117.2009.00416.x.
Wo, E., L. Song, T. Hurst, and N. Sitek, 2010, Geological review and bitumen resource appraisal of the Grosmont Formation within the Athabasca oil sands area: Presented at AAPG 2010 International Conference and Exhibition.
Yoon, T., 1986, Bitumen resources of the Upper Devonian Grosmont Formation: Twp 88 to 98, northern Alberta: Alberta Geological Survey open file report, 1986-01.
Zhao, Y., 2009, Petrophysical properties of bitumen from the Upper Devonian Grosmont reservoir, Alberta, Canada: M.S. thesis, University of Alberta.